The cryptic plastid of *Euglena longa* defines a new type of non-photosynthetic plastid organelles

Zoltán Füssy[1,2,3], Kristína Záhonová[1,2,4], Aleš Tomčala[1,*], Juraj Krajčovič[5], Vyacheslav Yurchenko[4], Miroslav Oborník[1,3], Marek Eliáš[4,#]

[1] Institute of Parasitology, Biology Centre ASCR, České Budějovice, Czech Republic

[2] Faculty of Science, Charles University, BIOCEV, Vestec, Czech Republic

[3] University of South Bohemia, Faculty of Science, České Budějovice, Czech Republic

[4] Life Science Research Centre, Department of Biology and Ecology and Institute of Environmental Technologies, Faculty of Science, University of Ostrava, Ostrava, Czech Republic

[5] Department of Biology, Faculty of Natural Sciences, University of ss. Cyril and Methodius in Trnava, Trnava, Slovakia

Running Head: Metabolic roles of the *Euglena longa* cryptic plastid

#Address correspondence to Marek Eliáš, marek.elias@osu.cz.

*Present address: University of South Bohemia, Faculty of Fisheries and Protection of Waters, CENAKVA, České Budějovice, Czech Republic

Zoltán Füssy and Kristína Záhonová contributed equally to this work. Author order was determined on the basis of seniority.

Word count:

Abstract: 395

Text: 6,277

Abstract

Most secondarily non-photosynthetic eukaryotes have retained residual plastids whose physiological role is often still unknown. One such example is *Euglena longa*, a close non-photosynthetic relative of *Euglena gracilis* harbouring a plastid organelle of enigmatic function. By mining transcriptome data from *E. longa* we finally provide an overview of metabolic processes localized to its elusive plastid. The organelle plays no role in biosynthesis of isoprenoid precursors and fatty acids, and has a very limited repertoire of pathways concerning nitrogen-containing metabolites. In contrast, the synthesis of phospholipids and glycolipids has been preserved, curiously with the last step of sulfoquinovosyldiacylglycerol synthesis being catalysed by the SqdX form of the enzyme so far known only from bacteria. Notably, we show that the *E. longa* plastid synthesizes tocopherols and a phylloquinone derivative, the first such report for non-photosynthetic plastids studied so far. The most striking attribute of the organelle is the presence of a linearized Calvin-Benson (CB) pathway including RuBisCO yet lacking the gluconeogenetic part of the standard cycle, together with ferredoxin-$NADP^+$ reductase (FNR) and the ferredoxin/thioredoxin systems. We hypothesize that FNR passes electrons to the ferredoxin/thioredoxin systems from NADPH to activate the linear CB pathway in response to the redox status of the *E. longa* cell. In effect, the pathway may function as a redox valve bypassing the glycolytic oxidation of glyceraldehyde-3-phosphate to 3-phosphoglycerate. Altogether, the *E. longa* plastid defines a new class of relic plastids that is drastically different from the best studied organelle of this category, the apicoplast.

Importance

Colourless plastids incapable of photosynthesis evolved in many plant and algal groups, but what functions they perform is still unknown in many cases. Here we study the elusive plastid of *Euglena longa*, a non-photosynthetic cousin of the familiar green flagellate *Euglena gracilis*. We document an unprecedented combination of metabolic functions that the *E. longa* plastid exhibits in comparison with previously characterized non-photosynthetic plastids. For example, and truly surprisingly, it has retained the synthesis of tocopherols (vitamin E) and a phylloquinone (vitamin K) derivative. In addition, we offer a possible solution of the long-standing conundrum of the presence of the CO_2-fixing enzyme RuBisCO in *E. longa*. Our work provides a detailed account on a unique variant of relic plastids, the first among non-photosynthetic plastids that evolved by secondary endosymbiosis from a green algal ancestor, and suggests that it has persisted for reasons not previously considered in relation to non-photosynthetic plastids.

Key words: Calvin-Benson cycle, *Euglena longa*, Euglenophyceae, evolution, non-photosynthetic plastids, phylloquinone, redox balance, sulfoquinovosyldiacylglycerol, tocopherol

INTRODUCTION

Photosynthesis was supposedly the primary evolutionary advantage driving the acquisition of the primary plastid as well as its further spread in eukaryotes by secondary and higher-order endosymbioses (1-3). However, plastids host many other metabolic pathways, such as biosynthesis of amino and fatty acids, isopentenyl pyrophosphate (IPP) and its derivatives (isoprenoids), and tetrapyrroles (4-6). Hence, reversion of photosynthetic lineages to heterotrophy typically does not entail plastid loss and non-photosynthetic plastids are found in many taxa (7-10).

The most extensively studied relic plastid is the apicoplast of apicomplexan parasites (*Plasmodium falciparum* and *Toxoplasma gondii*, above all). The essentiality of the apicoplast for parasite survival has attracted much attention as a promising target for parasite-specific inhibitors (11, 12). So far, three plastid pathways seem to condition the apicoplast retention: non-mevalonate IPP synthesis, haem synthesis, and type II fatty acid synthesis (FASII) (13). Less is known about plastid metabolic functions in other non-photosynthetic algal lineages. Many of them have a metabolic capacity similar to the apicoplast (10, 14, 15), but some house a more complex metabolism that includes amino acid biosynthesis and carbohydrate metabolism pathways (16-18). Until recently, IPP synthesis appeared to be a process conserved even in the most reduced plastids, such as the genome-lacking plastids of certain alveolates (8, 19). However, non-photosynthetic plastids lacking this pathway are now documented (9, 20, 21). Thus, there generally is a metabolic reason for plastid retention, although the cases of plastid dependency differ between lineages.

Like their prime representative *Euglena gracilis*, most euglenophytes are mixotrophs containing complex three-membrane-bound plastids derived from a green alga (22-24). Non-photosynthetic mutants of *E. gracilis* are capable of heterotrophic living (reviewed in 7, 25) and several euglenophyte lineages independently became secondarily heterotrophic (26). The best known is *Euglena* (previously *Astasia*) *longa*, a close relative of *E. gracilis* (26, 27). Although documentation at the cytological level is spurious (28-30), molecular sequence data provide clear evidence for the presence of a cryptic plastid organelle in this species. The *E. longa* plastid genome was sequenced two decades ago (31) and shown to lack all the photosynthesis-related genes, surprisingly except for *rbcL* encoding the large subunit of ribulose-1,5-bisphosphate carboxylase/oxygenase (RuBisCO). More recently, the existence of a nucleus-encoded small RuBisCO subunit (RBCS), synthesized as a precursor polyprotein, was documented in *E. longa*, although its processing into monomers could not be demonstrated (32). The physiological role of the *E. longa* RuBisCO and the whole plastid remains unknown, but indirect evidence suggests that the plastid is essential for *E. longa* survival (33-36).

To provide a resource for investigating the biology of *E. longa* and its plastid, we generated a

transcriptome assembly and demonstrated its high completeness and utility (37). We also showed that nucleus-encoded plastidial proteins in *E. longa* employ an N-terminal plastid-targeting bipartite topogenic signal (BTS) of the same two characteristic classes as known from *E. gracilis*. The *E. longa* transcriptome revealed unusual features of the plastid biogenesis machinery shared with photosynthetic euglenophytes, but also suggested specific reductions of housekeeping functions, reflecting the loss of photosynthesis (37). Nevertheless, the anabolic and catabolic pathways localized to the *E. longa* colourless plastid have not been characterized. Hence, we set to exploit the available sequence data to chart the metabolic map of the *E. longa* plastids. The analyses were greatly facilitated by the recent characterization of the *E. gracilis* plastid metabolic network based on a proteomic analysis of the organelle (38). Our study provides the first comprehensive view of a non-photosynthetic secondary plastid of green-algal origin and shows that the metabolic capacity of the *E. longa* plastid is strikingly different from those of the apicoplast and other relic plastids characterized in sufficient detail.

RESULTS

The plastid protein complement of *E. longa* is dramatically reduced compared to that its photosynthetic cousin

To obtain a global view of the repertoire of the plastid proteins in *E. longa*, we searched its transcriptome assembly to identify putative orthologs of the proteins defined as part of the *E. gracilis* plastid proteome (38). Of the 1,312 such proteins encoded by the *E. gracilis* nuclear genome, less than a half – namely 594 – exhibited an *E. longa* transcript that met our criteria for orthology (Table S1). As expected, the functional categories with the least proportion of putative *E. longa* orthologs included “photosynthesis”, “metabolism of cofactors and vitamins”, and “reaction to oxidative and toxic stress” with 95.89%, 85.11%, and 73.33% of proteins missing in *E. longa*. Interestingly, *E. longa* lacks counterparts also of some plastidial proteins involved in gene expression or genome maintenance, suggesting that the metabolic simplification, primarily the loss of photosynthesis itself with its high demand on protein turnover and mutagenic effects on the plastid genome, may have relaxed the constraints on the respective house-keeping molecular machineries.

Although these results clearly demonstrate dramatic reduction of the functional complexity of the *E. longa* plastid when compared to the plastid of its photosynthetic relative, they should not be interpreted such that the plastid harbours exactly the ~600 proteins identified by the orthology search. Firstly, the proteomically defined set of the putative *E. gracilis* plastid proteins is certainly affected by the presence of false negatives (bona fide plastid proteins missed by the analysis) as well as false positives (contaminants; (38). Secondly, orthology does not necessarily imply the same subcellular localization. Hence, to obtain a finer view of the physiological functions of the *E. longa* plastid, we systematically searched for homologs

of enzymes underpinning metabolic pathways known from plastids in general. N-terminal regions of the candidates were evaluated for characteristics of presequences predicting a specific subcellular localization to distinguish those likely representing plastid-targeted proteins from enzymes located in other compartments. Some of the bioinformatic predictions were further tested by biochemical analyses.

E. longa plastid lacks the MEP pathway of IPP biosynthesis, yet has kept the production of tocopherol and a phylloquinone derivative

There are two parallel pathways of IPP biosynthesis in *E. gracilis* (39): the mevalonate (MVA) pathway localized to the mitochondrion (first three enzymes) and the cytosol (the rest), and the plastid-localized 2-C-methyl-D-erythritol (MEP) pathway, the latter providing precursors for synthesis of terpenoid compounds connected to photosynthesis, namely carotenoids and plastoquinone (38, 39). As expected, only enzymes of the MVA pathway were found in *E. longa* (Table S2, Fig. 1a). The carotenoid and plastoquinone biosynthesis enzymes are all missing, but surprisingly the *E. longa* plastid appears still involved in terpenoid metabolism, specifically in its phytol branch.

Photosynthetic eukaryotes generally produce three types of phytol derivatives, tocopherols (vitamin E), phylloquinone (PhQ; vitamin K_1) and chlorophyll, starting with a common precursor phytyl-PP, which is (directly or indirectly *via* salvage of phytol liberated by chlorophyll degradation) made by reduction of geranylgeranyl-PP derived from the MEP pathway (40). *E. gracilis* proved to be unusual not only because it lacks the conventional geranylgeranyl-PP reductase (38), but also for making phytol from a precursor provided by the MVA pathway (39, 41). The route of phytol synthesis is currently unknown, though phytyl-PP might be synthesized in the *E. gracilis* plastid exclusively by the step-wise phosphorylation of phytol by phytol kinase (VTE5) and phytyl phosphate kinase (VTE6), enzymes employed in phytol salvage (38). *E. longa* has retained both VTE5 and VTE6, each being highly similar to their *E. gracilis* orthologs and exhibiting putative BTS (Fig. S1; Table S2). Since *E. longa* lacks chlorophyll and hence phytol recycling, these two enzymes are likely to participate in the *de novo* synthesis of phytol.

E. gracilis is known to make tocopherols and a PhQ derivative, 5'-monohydroxyphylloquinone (OH-PhQ; 38, 42, 43). All four enzymes mediating synthesis of α-tocopherol from phytyl-PP and homogentisate were identified and are localized to its plastid (38). Interestingly, their orthologs are found in *E. longa*, all with a typical BTS or at least with the N-terminal region being highly similar to the *E. gracilis* counterpart (Table S2), consistent with their presumed plastidial localization (Fig. 1a). Homogentisate itself is apparently made outside the plastid, as the enzyme responsible for its synthesis (4-hydroxyphenylpyruvate dioxygenase) is not found in the *E. gracilis* plastid proteome and the respective proteins have a predicted mitochondrial transit peptide in both *E. gracilis* and *E. longa* (Table S2). To test

the predicted ability of *E. longa* to produce α-tocopherol, we used HPLC-MS/MS to analyse extracts from this species and *E. gracilis* (grown at two different conditions – in light and in darkness) for comparison. Tocopherols were detected in both species (Fig. 1b), with α-tocopherol being the dominant form present in equivalent amounts in all three samples (Fig. 1c). The signals of β- and/or γ-tocopherol (indistinguishable by the method employed) and of δ-tocopherol suggest that tocopherol cyclase, and possibly also tocopherol O-methyltransferase, of both *Euglena* species can process substrates with or without the 3-methyl group on the benzene ring (Fig. S2).

The synthesis of OH-PhQ in *E. gracilis* is understood only partially, with only three enzymes of the pathway previously identified at the molecular level: the large multifunctional protein PHYLLO, apparently localized to the cytosol and catalysing the first four steps leading to o-succinylbenzoate; MenA, catalysing phytylation of dihydroxynaphthoate localized in the plastid; and MenG (demethylnaphthoquinone methyltransferase), possessing a typical BTS but not directly confirmed as plastidial by proteomics (38). Strikingly, *E. longa* expresses orthologs of these three *E. gracilis* proteins, all with the same predicted subcellular localization (Fig. 1a, Table S2). Like in *E. gracilis*, no candidates for other enzymes required for OH-PhQ synthesis could be identified by homology searches in *E. longa*. Still, OH-PhQ could be detected in this species (Fig. 1d, Fig. S3), although with a significantly lower abundance compared to that in *E. gracilis* (Fig. 1e).

***E. longa* plastid plays a limited role in the metabolism of nitrogen-containing compounds**

Some of the apparent peculiarities of the *E. longa* plastid do not stem from the loss of photosynthesis, but rather reflect unusual features of the plastid in euglenophytes in general. This particularly concerns plastid functions in the metabolism of nitrogen-containing compounds. Plastids are commonly involved in nitrogen assimilation due to housing nitrite reductase (44, 45), but *E. gracilis* cannot assimilate nitrate or nitrite (46, 47). Accordingly, no nitrite reductase can be identified in the transcriptome data from this species and *E. longa*. The plastids of both *Euglena* species apparently also lack the enzymes working immediately downstream of nitrite reductase, i.e. glutamine synthetase and glutamine oxoglutarate aminotransferase (the GS/GOGAT system common in plastids of other groups; 48, 49), indicating that the plastids rely on the import of organic nitrogen, similarly to what has been recently proposed for chromerids (50) and chrysophytes (20, 21).

A surprising feature of the *E. gracilis* plastid metabolism is the paucity of amino acid-related pathways (38). *E. longa* is even more extreme in this regard, because it lacks counterparts of the plastid-targeted serine biosynthesis enzymes. Thus, we could localize only two elements of amino acid biosynthesis pathways to the *E. longa* plastid (Fig. S4): serine/glycine hydroxymethyltransferase, whose apparent role is to provide the one-carbon moiety for formylmethionyl-tRNA synthesis required for the

plastidial translation; and one of the multiple isoforms of cysteine synthase A, which (like in *E. gracilis*) apparently relies on O-acetyl-L-serine synthesized outside of the plastid (see (38), and Table S3). This is not due to incompleteness of the sequence data, as the *E. longa* transcriptome encodes enzymes for the synthesis of all 20 proteinogenic amino acids, yet their predicted localization lies outside the plastid (Table S3).

Amino acids also serve as precursors or nitrogen donors for the synthesis of various other compounds in plastids (51, 52). This includes tetrapyrrole synthesis, which in *E. gracilis* is mediated by two parallel pathways localized to the mitochondrion/cytoplasm and the plastid (53). As described in detail elsewhere (Füssy, Záhonová, Oborník & Eliáš, unpublished), *E. longa* possesses the full mitochondrial-cytoplasmic pathway, whereas the plastidial one is restricted to its middle part potentially serving for synthesis of sirohaem, but not haem and chlorophyll (Fig. S4). The spectrum of reactions related to the metabolism of other nitrogen-containing cofactors or their precursors is very limited in the plastids of both *Euglena* spp. (Table S4). We identified only one such candidate in *E. longa* – vitamin B6 salvage catalysed by pyridoxamine 5'-phosphate oxidase, whereas *E. gracilis* additionally expresses two plastid-targeted isoforms of pyridoxine 4-dehydrogenase. Enzymes of *de novo* synthesis or salvage of purines and pyrimidines are also absent from the plastid of both *Euglena* species, except for a plastidial CTP synthase isoform in *E. gracilis* (supported by proteomic data), which is not expressed by *E. longa*. The lack of *in situ* CTP production may reflect the presumably less extensive synthesis of RNA and/or CDP-diacylglycerol (a precursor of phospholipids) in the *E. longa* plastid. Finally, *E. longa* expresses an ortholog of spermidine synthase found in the plastid proteome of *E. gracilis*, but it has a modified N-terminal sequence not fitting the characteristics of a BTS, suggesting a different subcellular localization. Nevertheless, both *E. longa* and *E. gracilis* have another homolog of this enzyme with an obvious BTS, so polyamines may be produced in the *E. longa* plastid after all (Fig. S4).

E. longa plastid does not make fatty acids but maintains phospholipid and glycolipid synthesis

Eukaryotes synthesize fatty acids by a single multi-modular fatty acid synthase I (FASI) in the cytosol or by a multi-enzyme type II fatty acid synthesis complex in the plastid. *E. gracilis* possesses both systems (54), but *E. longa* encodes only a homolog of the cytosolic FASI enzyme (Fig. 2a; Table S5). Nevertheless, *E. longa* still maintains plastid-targeted versions of acyl carrier protein (ACP) and 4'-phosphopantetheinyl transferases (or holo-ACP synthase), which are crucial for the synthesis of an active form of ACP (55). This is apparently employed by the predicted plastid-targeted homologs of acyl-ACP synthetases (presumably activating fatty acids imported into the plastid) and enzymes required for the synthesis of phosphatidic acid (PA) and its subsequent conversion to phosphatidylglycerol (PG) (Fig. 2a; Table S5). Notably, *E. longa* also has a parallel, plastid-independent, route of phosphatidylglycerol

synthesis (Table S6).

No other reactions of phospholipid synthesis or decomposition beyond PG synthesis seem to operate in the *E. longa* plastid. However, enzymes for the synthesis of galactolipids monogalactosyldiacylglycerol (MGDG) and digalactosyldiacylglycerol (DGDG) were identified, all with predicted BTSs (Fig. 2a, Table S5), consistent with the plastidial localization of galactolipid synthesis in other eukaryotes (56). Moreover, both MGDG and DGDG could be detected in *E. longa* and *E. gracilis* by HPLC-MS/MS, although galactolipid levels were significantly lower in *E. longa* than in *E. gracilis* (Fig. 2b). The presence of DGDG was further confirmed by immunofluorescence using an anti-DGDG antibody, which showed DGDG to be present in small foci in the *E. longa* cells (Fig. 2c), presumably representing individual small plastids. In comparison, extensive staining was observed in *E. gracilis* cells consistent with plastids occupying a large portion of the cytoplasm, whereas no staining was observed in the plastid-lacking euglenid *Rhabdomonas costata*.

We additionally identified another typical plastid glycolipid, sulfoquinovosyldiacylglycerol (SQDG; 57) in both *Euglena* spp. (Fig. 2b). The enzyme directly responsible for SQDG synthesis is sulfoquinovosyltransferase (Fig. 2a), but interestingly, its standard eukaryotic version (SQD2) is present only in *E. gracilis*, whereas both species share another isoform phylogenetically affiliated to bacterial SqdX (Fig. 3). To our knowledge, this is the first encounter of SqdX in any eukaryote. The presence of SQD2 only in *E. gracilis* may relate to the specific needs of its photosynthetic plastid. Indeed, *E. gracilis* contains much more SQDG compared to *E. longa* (Fig. 2b), and the profile of esterified fatty acids differs between the two species (*E. longa* lacks SQDG forms with unsaturated longer chains; Table S7).

The saccharide moieties of glycolipids in *E. longa* are probably also synthesized in its plastid (Fig. 2a). *E. longa* exhibits an ortholog of the *E. gracilis* UDP-glucose epimerase previously identified in the plastid proteome (Fig. S5, Table S5), explaining the source of UDP-galactose for galactolipid synthesis. This seems to be an original euglenozoan enzyme recruited into the plastid (Fig. S5), but, interestingly, *E. gracilis* encodes also a homolog of the unique plastidial UDP-glucose epimerase (PHD1) known from plants and various algae (58). The *E. gracilis* PHD1 possesses a predicted BTS (Table S5) and is thus also likely plastidial (albeit without proteomic support). This putative redundancy is not shared by *E. longa* (Fig. 2b) and may reflect a presumably much lower need for galactolipid synthesis. The origin of the SQDG precursor UDP-sulfoquinovose in *E. longa* remains obscure, because like *E. gracilis*, it lacks the conventional UDP-sulfoquinovose synthase SQD1/SqdB and probably employs an alternative, unrelated enzyme (38). UDP-glucose, i.e. the common precursor of both UDP-galactose and UDP-sulfoquinovose, may be produced directly in the plastid of *E. gracilis*, owing to the presence of an isoform of UDP-sugar pyrophosphorylase with a typical BTS (although absent among proteomically confirmed plastid proteins). *E. longa* lacks an ortholog of this protein as well as any other potentially plastidial enzyme of UDP-

glucose synthesis (Table S5), suggesting import of this metabolite from the cytosol.

E. longa plastid retains a linearized Calvin-Benson pathway

The expression of both subunits of RuBisCO in *E. longa* (32) raises the question whether the Calvin-Benson (CB) cycle (CBC) as a whole has been preserved in this organism. A putative *E. longa* plastid triose-phosphate isomerase was described previously (59), and we additionally identified homologs with putative BTSs for nearly all remaining CBC enzymes (Table S8). Phylogenetic analyses (supplementary dataset S1) showed specific relationships of the *E. longa* proteins to the previously characterized CBC enzymes from other euglenophytes (60). However, two key CBC enzymes are apparently missing from the *E. longa* transcriptome: phosphoglycerate kinase (ptPGK) and glyceraldehyde-phosphate dehydrogenase (ptGAPDH). Those homologs that are present are not orthologous to the plastid-targeted isoenzymes from other euglenophytes and all clearly lack a BTS (Table S8). Hence, these are presumably cytosolic enzymes involved in glycolysis/gluconeogenesis. The lack of ptPGK and ptGAPDH in *E. longa* implies that the product of the RuBisCO carboxylase activity, 3-phosphoglycerate (3PG), cannot be converted (*via* 1,3-bisphosphoglycerate; 1,3-BPG) to glyceraldehyde-3-phosphate (GA3P) in the plastid (Fig. 4a).

Assuming that the reactions catalysed by fructose bisphosphatase, phosphoribulokinase, and RuBisCO are irreversible (61), the flux through this linearized CB pathway goes from GA3P to 3PG, with a net production of six molecules of 3PG from five molecules of GA3P due to fixation of three CO_2 molecules catalysed by RuBisCO. Euglenophytes do not store starch in the plastid (62), and indeed, we did not find any glucose metabolism-related enzymes with a BTS in *E. longa*. Hence, GA3P cannot be produced by a glycolytic route in the *E. longa* plastid. The presence of the plastid-targeted glycerol-3-phosphate dehydrogenase (Table S5) in principle allows for generation of GA3P from glycerol-3-phosphate (*via* dihydroxyacetone phosphate; DHAP; Fig. 2), which could possibly come from glycerolipids turnover, but no plastidial phospholipid-degradation enzymes were found in *E. longa*. Hence, the primary function of glycerol-3-phosphate dehydrogenase perhaps is to provide glycerol-3-phosphate for the plastid phospholipid and glycolipid synthesis (see above) and the *E. longa* plastid most likely imports GA3P or DHAP from the cytosol (Fig. 4a). This assumption is supported by the presence of several members of the plastid phosphate translocator (pPT) family (Fig. S6; 63), including one phylogenetically closest to a cryptophyte transporter with a preference for DHAP (64). Concerning the opposite end of the linear CB pathway, we did not identify any *E. longa* plastid-targeted enzyme that would metabolize 3PG further, suggesting that this intermediate is exported from the plastid into the cytosol, probably also by one of the pPT transporters (Fig. 4a).

RuBisCO is not only a carboxylase, but also exhibits an oxygenase activity catalysing the

298 production of phosphoglycolate, which is then recycled by the photorespiration pathway; this is initiated
299 by phosphoglycolate phosphatase, yielding glycolate (65). Indeed, *E. longa* contains an ortholog of the *E.*
300 *gracilis* plastidial phosphoglycolate phosphatase (Table S8), but in contrast to *E. gracilis* no homolog of
301 the glycolate transporter PLGG1 mediating glycolate export from the plastid (66) was found in *E. longa*
302 (Table S8). Since it also lacks obvious candidates for plastid-targeted glycolate-metabolizing enzymes
303 (glycolate oxidase, glyoxylate reductase, glycolaldehyde dehydrogenase, glyoxylate
304 carboligase/tartronate-semialdehyde reductase), it is unclear how glycolate is removed from the *E. longa*
305 plastid. Possibly the amount of glycolate produced is low and can be exported by an uncharacterized
306 PLGG1-independent route that exists also in plant plastids (67) and is sufficient for glycolate recycling in
307 the semi-parasitic plant *Cuscuta campestris* (68).
308
309 **_E. longa_ plastid preserves the redox regulatory system of the CB pathway**
310 Although the photosynthetic machinery is missing from *E. longa* (37), we found homologs (with clear
311 plastidial localization) of the typical "photosynthetic" (PetF-related) ferredoxin (Fd) and ferredoxin-
312 $NADP^+$ reductase (FNR) (Table S9). These two proteins are primarily involved in passing electrons from
313 activated photosystem I to $NADP^+$. Euglenophyte FNR homologs belong to two different, yet related,
314 clades (Fig. 5). One comprises the *E. longa* FNR plus its orthologs from photosynthetic euglenophytes,
315 whereas the second one is restricted to the photosynthetic species. Two different FNR forms also exist in
316 plants (Fig. 5), one functioning in photosynthesis (photosystem I-dependent production of NADPH) and
317 the other "non-photosynthetic" one, allowing electron flow in the reverse direction, from NADPH to Fd
318 (69). In analogy, we suggest that the two euglenophyte FNR forms functionally differ, one serving in
319 photosynthesis and the other, present also in *E. longa*, mediating light-independent production of the
320 reduced Fd. Multiple plastid anabolic enzymes depend on reduced Fd as an electron donor (4), but none of
321 them seems to account for the presence of FNR and Fd in the *E. longa* plastid: glutamate synthase and
322 nitrite reductase are missing, all identified lipid desaturases are predicted as mitochondrion- or ER-
323 targeted (Table S5) and sulfite reductase, like the one previously identified in the plastid of *E. gracilis*
324 (38), is NADPH-dependent (Table S5).
325 Fd also provides electrons to ferredoxin:thioredoxin reductase (FTR) mediating reduction of the
326 protein thioredoxin (Trx). The Fd/Trx system regulates several CBC enzymes in response to the stromal
327 redox status, whereby an excess of NADPH leads to electrons being relayed from Fd *via* Trx to certain
328 disulfide bonds in the target enzymes to activate them (Fig. 4a; 70). Notably, FTR and Trx homologs with
329 an evident BTS are present in *E. longa* (Table S9), and specific motifs necessary for the function of the
330 Fd/Trx system are conserved in the respective *E. longa* proteins (Fig. S7). In addition, three *E. longa* CBC
331 enzymes, fructose bisphosphatase (two of the three isoforms present), sedoheptulose bisphosphatase, and

phosphoribulokinase, exhibit the conserved Trx regulatory cysteine motifs, similar to their orthologs in *E. gracilis* (Fig. S7, Table S10). Thus, the *E. longa* CB pathway is likely to be sensitive to the redox status in the plastid, specifically to the concentration of NADPH (Fig. 4a).

DISCUSSION

The analyses described above provide evidence for the cryptic *E. longa* plastid harbouring highly non-conventional combination of metabolic functions. Lacking the plastidial MEP pathway, *E. longa* joins the only recently discovered group of plastid-bearing eukaryotes with such a deficit, namely the colourless diatom *Nitzschia* sp. NIES-3581 (9) and various colourless chrysophytes (20, 21). An obvious explanation for this is that the cytosolic MVA pathway is sufficient to supply precursors for all cellular isoprenoids in these organisms. In contrast, the MEP pathway in apicomplexans and related alveolates (i.e. Myzozoa; 8), and in diverse non-photosynthetic chlorophytes (71), is essential, since the cytosolic MVA pathway was lost in these groups (72, 73). Strikingly, the *E. longa* plastid is still involved in isoprenoid metabolism, namely the synthesis of tocopherols and OH-PhQ. Like in *E. gracilis*, pathway leading to OH-PhQ cannot be presently reconstructed in full detail in either *Euglena* spp. (see also 38). Both euglenophytes studied lack homologs of the conventional enzymes of the middle part of the pathway (from *o*-succinylbenzoate to dihydroxynaphthoate) typically localized in the peroxisome (74). The respective enzyme activities were found associated with the plastid envelope in *E. gracilis* (75), suggesting an alternative solution that may hold for *E. longa*, too. The molecular identity of the putative PhQ hydroxylase (making OH-PhQ) is unknown, so its plastidial localization in *E. gracilis* or *E. longa* cannot be ascertained. Finally, a previously unknown step – reduction of the naphthoquinone ring – was demonstrated as a prerequisite for the reaction catalysed by MenG to proceed in plants and cyanobacteria (76). The respective reductase is well conserved among diverse cyanobacteria, algae and plants (74), but we did not identify close homologs in any of the euglenophyte transcriptome assemblies, suggesting that euglenophytes employ an unknown alternative enzyme.

E. longa seems to be the first eukaryote with a non-photosynthetic plastid documented to have retained the pathways for tocopherols and OH-PhQ synthesis. The presence of tocopherols in *E. longa* is not that surprising, as they are not restricted to photosynthetic tissues in plants and were detected also in non-photosynthetic *E. gracilis* mutants (42, 77). As potent lipophilic antioxidants, tocopherols might be employed by *E. longa* to protect its membrane lipids against reactive oxygen species generated by mitochondria and peroxisomes. The retention of OH-PhQ synthesis in *E. longa* is more puzzling, as the best-established role of (OH-)PhQ in plants and algae is its functioning as an electron carrier within the photosystem I (43, 78). PhQ was additionally proposed to serve as an electron acceptor required for proper function of photosystem II (79, 80). A homolog of the respective oxidoreductase (LTO1) is present in *E.*

366 *gracilis* (Table S2), but not in the transcriptomic data from *E. longa*. Interestingly, in plants PhQ was also
367 detected in the plasma membrane and proposed to be involved in photosynthesis-unrelated redox
368 processes (81-83). However, the MenA and MenG enzymes in *E. longa* carry a typical BTS, so we
369 suggest that OH-PhQ in *E. longa* is involved in a hitherto uncharacterized, photosynthesis-unrelated
370 plastid-resident process.

371 The absence of the type II fatty acid synthesis in the *E. longa* plastid is noteworthy, yet not
372 unprecedented, since it has been also reported for the non-photosynthetic plastids of certain myzozoans (8)
373 and a chrysophyte (20). Still, the *E. longa* plastid plays an active role in the lipid metabolism, having
374 retained biosynthesis of several glycerolipid types, including galactolipids and SQDG. These were
375 previously documented in several non-photosynthetic algae, e.g. colourless diatoms (84, 85). On the other
376 hand, the apicoplast (86, 87), and most likely also the relic plastid of *Helicosporidium* (based on our
377 analysis of the respective genome data reported by 17), lack galactolipid and SQDG synthesis completely.
378 The reason for the differential retention of these lipids in different colourless plastids remains to be
379 investigated further.

380 The truly striking feature of the *E. longa* plastid is the retention of nearly all CBC enzymes
381 (assembling a putative linear CB pathway) and the mechanism of their redox regulation. In fact, the
382 presence of CBC enzymes have been reported from a set of unrelated colourless algae and plants. Some of
383 them, e.g. the dinoflagellate *Crypthecodinium cohnii*, dictyochophytes *Pteridomonas danica* and
384 *Ciliophrys infusionum*, the cryptophyte *Cryptomonas paramecium*, and some parasitic or
385 mycoheterotrophic land plants, are known to encode RuBisCO (7, 15, 88-90), but the actual complement
386 of other CBC enzymes in these species is unknown. In contrast, transcriptomic or genomic analyses of
387 other colourless plastid-bearing taxa, such as the dinoflagellate *Pfiesteria piscicida*, the chlorophyte
388 *Helicosporidium* sp. ATCC50920, the diatom *Nitzschia* sp. NIES-3581, and the non-photosynthetic
389 chrysophytes, revealed the presence of a subset of CBC enzymes, including ptPGK and ptGAPDH, but
390 not of RuBisCO (9, 17, 21, 91). Hence, the constellation of the CBC enzymes present in the *E. longa*
391 plastid is unique.

392 The CBC enzymes retained in various non-photosynthetic eukaryotes obviously do not serve to
393 sustain autotrophic growth due to lack of photosynthetic production of ATP and NADPH. The incomplete
394 CBC in *Nitzschia* was proposed to provide erythrose-4-P for the synthesis of aromatic amino acid *via* the
395 shikimate pathway (9). The data provided for the *Helicosporidium* plastid (17) offer the same explanation
396 of the retention of several CBC enzyme. However, such rationalization cannot hold for *E. longa*, since
397 aromatic amino acid biosynthesis in this species apparently localizes to the cytosol (Table S3) and thus
398 has an access to erythrose-4-P produced by the pentose phosphate pathway. In addition, *E. longa* differs
399 from both *Nitzschia* and *Helicosporidium* by the retention of RuBisCO. A photosynthesis- and CBC-

independent role of RuBisCO was described in oil formation in developing seeds of *Brassica napus*, where refixation of CO_2 released during carbohydrate-to-fatty acid conversion increases carbon use efficiency (92). The absence of fatty acid synthesis in the *E. longa* plastid makes a similar function of RuBisCO unlikely in this organism.

The identification of the Fd/Trx system in the *E. longa* plastid, despite the absence of photosynthesis, may thus be a key for understanding the physiological role of the linear CB pathway in *E. longa*. Another hint is provided by the discovery of a unique (non-phosphorylating) form of GAPDH, referred to as GapN, in the *E. gracilis* plastid (38). This enzyme uses $NADP^+$ to directly oxidize GA3P to 3PG without ATP generation (93). In plants, GapN is cytosolic and involved in shuttling of reducing equivalents from the plastid by the exchange of GA3P and 3PG between the two compartments (94). *E. longa* possesses a protein orthologous to the *E. gracilis* GapN with predicted BTS (Table S8), suggesting its plastidial localization. It thus appears that in *Euglena* spp., GapN mediates shuttling of reducing equivalents in the opposite direction than in plants, i.e. from the cytosol to the plastid (Fig. 4a). In case of *E. longa* this may be the main (if not the only) mechanism of providing NADPH for the use in the plastid, whereas *E. gracilis* would utilize it when photosynthetic NADPH production is shut down. At the same time, the shuttle provides a mechanism of linking the level of NADPH in the plastid with the cytosolic concentration of GA3P.

Taken together, we propose that in *E. longa* (and, at specific circumstances, possibly also in *E. gracilis*), the plastidial NADPH/$NADP^+$ ratio is directly influenced by the redox status of the cell, i.e. that it rises in an excess of reducing power that slows down the glycolytic oxidation of GA3P in the cytosol. This stimulates the linear CB pathway *via* the Fd/Trx system, effectively decreasing the level of GA3 by converting it to 3PG without further increasing the reducing power in the cell. This conclusion is apparent from considering the overall stoichiometries of the two alternative pathways from GA3 to 3PG (Fig. 4b). The key difference is that the CB pathway does not produce NADH that needs to be reoxidized to keep the glycolytic pathway running, since the fixed CO_2 effectively serves as an electron acceptor. Hence, turning the CB bypass on may help the cell to keep the redox balance when reoxidation of NADH is not efficient, e.g. at hypoxic (or anoxic) conditions (although this happens at the expense of ATP). Indeed, euglenophytes in their natural settings are probably often exposed to the shortage of oxygen, and anaerobiosis in *E. gracilis* has been studied to some extent (54, 95). The anaerobic heterotrophic metabolism of *E. gracilis* relies on fermentative degradation of paramylon leading to production of wax esters (96). It is likely that *E. longa* exhibits a similar metabolic adaptation to low oxygen levels as *E. gracilis*. However, details of the euglenophyte anaerobic metabolism need to be investigated further, and we propose that the plastid may be involved in it as a "redox valve".

Compared to the range of forms mitochondria may exhibit in diverse eukaryotes (97), plastids

seem to be much more uniform. However, this is partly a reflection of our ignorance about plastid biology in most algal groups, and recent studies of various independently evolved colourless plastids document a surprising degree of diversity in terms of their metabolic capacity. Our analyses of the *E. longa* plastid stretch the breadth of variation among non-photosynthetic plastids even further. The combination of pathways present (tocopherol and phylloquinone synthesis, glycolipid synthesis and a linearized CB pathway including RuBisCO), absent (fatty acid, amino acid, and isoprenoid precursor synthesis), and truncated (tetrapyrrole synthesis; Füssy, Záhonová, Oborník & Eliáš, unpublished) makes the *E. longa* plastid unlike any of the previously investigated non-photosynthetic plastids, including the apicoplast. However, further work, combining additional *in silico* analyses (aimed, e.g., at potential plastid membrane transporters mediating metabolite exchange with the cytosol) with biochemical and cytological investigations is needed to achieve a more precise idea about the protein composition of the *E. longa* plastid and a better understanding of its physiological roles.

MATERIALS AND METHODS

Identification and annotation of plastid-targeted proteins

The analyses utilized the *E. longa* transcriptome assembly reported previously, with candidates for plastid-targeted proteins identified as described in (37), including careful manual curation of the sequences and, if needed, revision of the 5'-ends of the transcripts by targeted searches of unassembled sequencing reads. Protein models with a putative BTS were automatically annotated using InterProScan 5.21 (98). Potential plastid enzymes (references from the KEGG PATHWAY Database, https://www.genome.jp/kegg/pathway.html) or sequences identified by literature searches, and plastid proteins identified by (38) were searched using BLAST v.2.2.30 (against the conceptually translated proteome, the transcriptome assembly and RNA-seq reads). HMMER 3.0 (99) was used when BLAST did not yield expected candidate homologs. For comparative purposes we used the same approach to identify plastid-targeted proteins encoded by the transcriptome assemblies from *E. gracilis* reported by (96) (accession GDJR00000000.1) and (100) (accession GEFR00000000.1).

To identify orthologs of the proteins from *E. gracilis* plastid proteome (38) in *E. longa*, these were used as queries in reciprocal BLAST searches. Briefly, *E. gracilis* proteins identified in its plastid proteome were used as queries in tBLASTn searches in *E. longa* transcriptome with E-value cut-off 0.1. Each respective best BLAST hit from *E. longa* was then used as a query to search the whole *E. gracilis* transcriptomic database and was classified as an ortholog if it retrieved the original *E. gracilis* query as a first hit. Results are summarized in Table S1.

For MenA cDNA resequencing, mRNA was extracted using the TRI Reagent and Dynabeads mRNA Purification kit (both from Thermo Fisher Scientific, Waltham, USA). Reverse-transcription was

performed with random hexamers and StrataScript III Reverse Transcriptase (Thermo Fisher Scientific). The target was amplified using forward 5'-GGTGCTGTTCTGCTCTCACT-3' and reverse 5'-CAGTGGGGATCAGAGATGCG-3' primers, and Q5 High-Fidelity DNA polymerase in a standard buffer (New England Biolabs, Ipswich, USA). Amplicons were purified on MinElute PCR Purification columns (Qiagen, Hilden, Germany) and sequenced at the GATC sequencing facility (Konstanz, Germany). The MenA cDNA sequence is deposited in GenBank (MK484704).

Phylogenetic analyses

Homologs of target proteins were identified by BLAST v.2.2.30 searches in the non-redundant protein sequence database at NCBI (www.ncbi.nlm.nih.gov) and among protein models of selected organisms from JGI (jgi.doe.gov) and MMETSP (marinemicroeukaryotes.org; 101). Datasets were processed using an in-house script (https://github.com/morpholino/Phylohandler) as follows. Sequences were aligned using the MAFFT v7.407 tool with L-INS-I setting (102) and poorly aligned positions were eliminated using trimAl v1.4.rev22 with "-automated1" trimming (103). For presentation purposes, alignments were processed using CHROMA (104). Maximum likelihood trees were inferred using the LG+F+G4 model of IQ-TREE v1.6.9 (105), employing the strategy of rapid bootstrapping followed by a "thorough" likelihood search with 1,000 bootstrap replicates. The list of species, and the number of sequences and amino acid positions are present in Tables S11-S22 for each phylogenetic tree.

Culture conditions

Euglena gracilis strain *Z* ("autotrophic" conditions) was cultivated statically under constant illumination at 26 °C in Cramer-Myers medium with ethanol (0.8% v/v) as a carbon source (106). *E. longa* strain CCAP 1204-17a (a gift from Wolfgang Hachtel, Bonn, Germany) and heterotrophic *E. gracilis* strain *Z* were cultivated as above, but without illumination. *Rhabdomonas costata* strain PANT2 (a gift from Vladimír Hampl, Charles University, Prague, Czech Republic) was isolated from a freshwater body in Pantanal (Brazil) and grown with an uncharacterised mixture of bacteria in Sonneborn's *Paramecium* medium, pH 7.4 (107) at room temperature.

Mass spectrometry of structural lipids and terpenoids

Lipid extracts from *E. longa* and autotrophically grown *E. gracilis* cellular pellets (four biological samples of different culture ages) were obtained with procedures described in (108). Briefly, approximately 10 mg (wet weight) of both harvested cultures were homogenized by using a TissueLyser LT mill (Qiagen) and extraction was performed by chloroform and methanol solution (ratio – 2:1) following the previously described method (109). Aliquots from each sample were subjected to HPLC MS system powered by a

linear ion trap LTQ-XL mass spectrometer (Thermo Fisher Scientific). The settings of the system followed the methodology published earlier (108). Data were acquired and processed using Xcalibur software version 2.1 (Thermo Fisher Scientific). Particular compounds were determined based on earlier publication (108). Terpenoids were extracted from an autotrophic and heterotrophic culture of *E. gracilis*, and a culture of *E. longa* of the same age in three replicates. The same extraction protocol as for lipid analysis was used. Sample aliquots were injected into the high-resolution mass spectrometry system powered by Orbitrap Q-Exactive Plus with Dionex Ultimate 3000 XRS pump and Dionex Ultimate 3000 XRS Open autosampler (both from Thermo Fisher Scientific) and followed the settings described in (108). Data were acquired and processed using Xcalibur software version 2.1. Identification of OH-PhQ was done by considering the m/z value, fragmentation pattern, and high-resolution data. Tocopherols (α, β/γ, and δ) were determined by the same characteristics as OH-PhQ and results were then compared with commercially purchased standards (Sigma-Aldrich, St. Louis, USA).

Immunofluorescence assay

Immunofluorescence was performed as described previously (110). Briefly, cells were fixed in 4% paraformaldehyde for 30 minutes, permeabilized for 10 minutes on ice with 0.1% Igepal CA-630 (Sigma-Aldrich) in PHEM buffer pH 6.9 (60 mM PIPES, 25 mM HEPES, 10 mM EGTA, 2 mM $MgCl_2$), and background was masked with 3% BSA in PHEM buffer. DGDG was detected using a polyclonal rabbit anti-DGDG antibody (1:25), a kind gift from Cyrille Y. Botté (University of Grenoble I, Grenoble, France), followed by incubation with a secondary Cy3-labeled polyclonal goat anti-rabbit antibody (AP132C, 1:800, Merck Millipore, Burlington, USA). Cells were mounted on slides using Fluoroshield™ with DAPI mounting medium (Sigma-Aldrich) and observed with an Olympus BX53 microscope (Olympus, Tokyo, Japan).

ACKNOWLEDGEMENTS

We thank Vladimír Hampl for the culture of *Rhabdomonas costata* and Cyrille Y. Botté for the anti-DGDG antibody. We acknowledge the infrastructure grant "Přístroje IET" (CZ.1.05/2.1.00/19.0388). Computational resources were supplied by the Ministry of Education, Youth and Sports of the Czech Republic under the Projects CESNET (Project No. LM2015042) and CERIT-Scientific Cloud (Project No. LM2015085) provided within the program Projects of Large Research, Development and Innovations Infrastructures. We thank Laboratory of Analytical Biochemistry and Metabolomics (Biology Centre ASCR) for an access to LC–MS instruments. This study was supported by the Czech Science Foundation grants 17-21409S (to ME) and 18-13458S (to MO), ERD Funds (the project CePaViP; CZ.02.1.01/0.0/0.0/16_019/0000759) and the Scientific Grant Agency of the Slovak Ministry of

Education (grant VEGA 1/0535/17 to JK).

REFERENCES

1. Keeling PJ. 2013. The number, speed, and impact of plastid endosymbioses in eukaryotic evolution. Annu Rev Plant Biol 64:583-607.
2. McFadden GI. 2014. Origin and evolution of plastids and photosynthesis in eukaryotes. Cold Spring Harb Perspect Biol 6:a016105.
3. Ponce-Toledo RI, Deschamps P, Lopez-Garcia P, Zivanovic Y, Benzerara K, Moreira D. 2017. An early-branching freshwater cyanobacterium at the origin of plastids. Curr Biol 27:386-391.
4. Neuhaus HE, Emes MJ. 2000. Nonphotosynthetic metabolism in plastids. Annu Rev Plant Physiol Plant Mol Biol 51:111-140.
5. Oborník M, Green BR. 2005. Mosaic origin of the heme biosynthesis pathway in photosynthetic eukaryotes. Mol Biol Evol 22:2343-53.
6. Van Dingenen J, Blomme J, Gonzalez N, Inzé D. 2016. Plants grow with a little help from their organelle friends. J Exp Bot 67:6267-6281.
7. Hadariová L, Vesteg M, Hampl V, Krajčovič J. 2018. Reductive evolution of chloroplasts in non-photosynthetic plants, algae and protists. Curr Genet 64:365-387.
8. Janouškovec J, Tikhonenkov DV, Burki F, Howe AT, Kolísko M, Mylnikov AP, Keeling PJ. 2015. Factors mediating plastid dependency and the origins of parasitism in apicomplexans and their close relatives. Proc Natl Acad Sci U S A 112:10200-7.
9. Kamikawa R, Moog D, Zauner S, Tanifuji G, Ishida KI, Miyashita H, Mayama S, Hashimoto T, Maier UG, Archibald JM, Inagaki Y. 2017. A non-photosynthetic diatom reveals early steps of reductive evolution in plastids. Mol Biol Evol 34:2355-2366.
10. Slamovits CH, Keeling PJ. 2008. Plastid-derived genes in the nonphotosynthetic alveolate *Oxyrrhis marina*. Mol Biol Evol 25:1297-306.
11. McFadden GI, Yeh E. 2017. The apicoplast: now you see it, now you don't. Int J Parasitol 47:137-144.
12. Miller LH, Ackerman HC, Su XZ, Wellems TE. 2013. Malaria biology and disease pathogenesis: insights for new treatments. Nat Med 19:156-67.
13. Lim L, McFadden GI. 2010. The evolution, metabolism and functions of the apicoplast. Philos Trans R Soc Lond B Biol Sci 365:749-63.
14. Fernández Robledo JA, Caler E, Matsuzaki M, Keeling PJ, Shanmugam D, Roos DS, Vasta GR. 2011. The search for the missing link: a relic plastid in *Perkinsus*? Int J Parasitol 41:1217-29.
15. Sanchez-Puerta MV, Lippmeier JC, Apt KE, Delwiche CF. 2007. Plastid genes in a non-

570 photosynthetic dinoflagellate. Protist 158:105-17.
571 16. Borza T, Popescu CE, Lee RW. 2005. Multiple metabolic roles for the nonphotosynthetic plastid of
572 the green alga *Prototheca wickerhamii*. Eukaryot Cell 4:253-61.
573 17. Pombert JF, Blouin NA, Lane C, Boucias D, Keeling PJ. 2014. A lack of parasitic reduction in the
574 obligate parasitic green alga *Helicosporidium*. PLoS Genet 10:e1004355.
575 18. Smith DR, Lee RW. 2014. A plastid without a genome: evidence from the nonphotosynthetic green
576 algal genus *Polytomella*. Plant Physiol 164:1812-9.
577 19. Matsuzaki M, Kuroiwa H, Kuroiwa T, Kita K, Nozaki H. 2008. A cryptic algal group unveiled: a
578 plastid biosynthesis pathway in the oyster parasite *Perkinsus marinus*. Mol Biol Evol 25:1167-79.
579 20. Dorrell RG, Azuma T, Nomura M, Audren de Kerdrel G, Paoli L, Yang S, Bowler C, Ishii KI,
580 Miyashita H, Gile GH, Kamikawa R. 2019. Principles of plastid reductive evolution illuminated by
581 nonphotosynthetic chrysophytes. Proc Natl Acad Sci U S A 116:6914-6923.
582 21. Graupner N, Jensen M, Bock C, Marks S, Rahmann S, Beisser D, Boenigk J. 2018. Evolution of
583 heterotrophy in chrysophytes as reflected by comparative transcriptomics. FEMS Microbiol Ecol 94.
584 22. Jackson C, Knoll AH, Chan CX, Verbruggen H. 2018. Plastid phylogenomics with broad taxon
585 sampling further elucidates the distinct evolutionary origins and timing of secondary green plastids.
586 Sci Rep 8:1523.
587 23. Leander BS, Esson HJ, Breglia SA. 2007. Macroevolution of complex cytoskeletal systems in
588 euglenids. Bioessays 29:987-1000.
589 24. Turmel M, Gagnon MC, O'Kelly CJ, Otis C, Lemieux C. 2009. The chloroplast genomes of the green
590 algae *Pyramimonas*, *Monomastix*, and *Pycnococcus* shed new light on the evolutionary history of
591 prasinophytes and the origin of the secondary chloroplasts of euglenids. Mol Biol Evol 26:631-48.
592 25. Krajčovič J, Ebringer L, Schwartzbach SD. 2002. Reversion of endosymbiosis?, p 185-206. *In*
593 Seckbach J (ed), Symbiosis: Mechanisms and model systems doi:10.1007/0-306-48173-1_11.
594 Springer Netherlands, Dordrecht.
595 26. Marin B, Palm A, Klingberg M, Melkonian M. 2003. Phylogeny and taxonomic revision of plastid-
596 containing euglenophytes based on SSU rDNA sequence comparisons and synapomorphic signatures
597 in the SSU rRNA secondary structure. Protist 154:99-145.
598 27. Nudelman MA, Rossi MS, Conforti V, Triemer RE. 2003. Phylogeny of Euglenophyceae based on
599 small subunit rDNA sequences: Taxonomic implications. J Phycol 39:226-235.
600 28. Hachtel W. 1996. DNA and gene expression in nonphotosynthetic plastids, p 349-355. *In* Pessarakli
601 M (ed), Handbook of Photosynthesis. Marcel Dekker, New York.
602 29. Kivic PA, Vesk M. 1974. An electron microscope search for plastids in bleached *Euglena gracilis*
603 and in *Astasia longa*. Can J Bot 52:695-699.

30. Webster DA, Hackett DP, Park RB. 1967. The respiratory chain of colorless algae: III. Electron microscopy. J Ultrastruct Res 21:514-523.
31. Gockel G, Hachtel W. 2000. Complete gene map of the plastid genome of the nonphotosynthetic euglenoid flagellate *Astasia longa*. Protist 151:347-51.
32. Záhonová K, Füssy Z, Oborník M, Eliáš M, Yurchenko V. 2016. RuBisCO in non-photosynthetic alga *Euglena longa*: divergent features, transcriptomic analysis and regulation of complex formation. PLoS One 11:e0158790.
33. Gockel G, Hachtel W, Baier S, Fliss C, Henke M. 1994. Genes for components of the chloroplast translational apparatus are conserved in the reduced 73-kb plastid DNA of the nonphotosynthetic euglenoid flagellate *Astasia longa*. Curr Genet 26:256-62.
34. Hadariová L, Vesteg M, Birčák E, Schwartzbach SD, Krajčovič J. 2017. An intact plastid genome is essential for the survival of colorless *Euglena longa* but not *Euglena gracilis*. Curr Genet 63:331-341.
35. Siemeister G, Buchholz C, Hachtel W. 1990. Genes for ribosomal proteins are retained on the 73 kb DNA from *Astasia longa* that resembles *Euglena* chloroplast DNA. Curr Genet 18:457-64.
36. Siemeister G, Buchholz C, Hachtel W. 1990. Genes for the plastid elongation factor Tu and ribosomal protein S7 and six tRNA genes on the 73 kb DNA from *Astasia longa* that resembles the chloroplast DNA of *Euglena*. Mol Gen Genet 220:425-32.
37. Záhonová K, Füssy Z, Birčák E, Novák Vanclová AMG, Klimeš V, Vesteg M, Krajčovič J, Oborník M, Eliáš M. 2018. Peculiar features of the plastids of the colourless alga *Euglena longa* and photosynthetic euglenophytes unveiled by transcriptome analyses. Sci Rep 8:17012.
38. Novák Vanclová AMG, Zoltner M, Kelly S, Soukal P, Záhonová K, Füssy Z, Ebenezer TE, Lacová Dobáková E, Eliáš M, Lukeš J, Field M, Hampl V. 2019. Metabolic quirks and the colourful history of the *Euglena gracilis* secondary plastid. New Phytologist accepted.
39. Kim D, Filtz MR, Proteau PJ. 2004. The methylerythritol phosphate pathway contributes to carotenoid but not phytol biosynthesis in *Euglena gracilis*. J Nat Prod 67:1067-9.
40. Gutbrod K, Romer J, Dormann P. 2019. Phytol metabolism in plants. Prog Lipid Res 74:1-17.
41. Disch A, Schwender J, Muller C, Lichtenthaler HK, Rohmer M. 1998. Distribution of the mevalonate and glyceraldehyde phosphate/pyruvate pathways for isoprenoid biosynthesis in unicellular algae and the cyanobacterium *Synechocystis* PCC 6714. Biochem J 333 (Pt 2):381-8.
42. Watanabe F, Yoshimura K, Shigeoka S. 2017. Biochemistry and physiology of vitamins in *Euglena*, p 65-90. *In* Schwartzbach SD, Shigeoka S (ed), *Euglena*: Biochemistry, cell and molecular biology, vol 979. Springer International Publishing, Cham.
43. Ziegler K, Maldener I, Lockau W. 1989. 5'-monohydroxyphylloquinone as a component of

638 photosystem I. Zeitschrift für Naturforschung C 44:468-472.
639 44. Giordano M, Raven JA. 2014. Nitrogen and sulfur assimilation in plants and algae. Aquatic Botany
640 118:45-61.
641 45. Sanz-Luque E, Chamizo-Ampudia A, Llamas A, Galvan A, Fernandez E. 2015. Understanding
642 nitrate assimilation and its regulation in microalgae. Front Plant Sci 6:899.
643 46. Kitaoka S, Nakano Y, Miyatake K, Yokota A. 1989. Enzymes and their functional location, p 1-135.
644 *In* Buetow DE (ed), Subcellular biochemistry and molecular biology
645 doi:https://doi.org/10.1016/B978-0-12-139904-7.50007-5. Academic Press.
646 47. Oda Y, Miyatake K, Kitaoka S. 1979. Inability of *Euglena gracilis Z* to utilize nitrate, nitrite and urea
647 as the nitrogen sources. Bulletin of the University of Osaka Prefecture Series B Agriculture and
648 Biology 31:43-48.
649 48. Dagenais-Bellefeuille S, Morse D. 2013. Putting the N in dinoflagellates. Front Microbiol 4:369.
650 49. Fernandez E, Galvan A. 2008. Nitrate assimilation in *Chlamydomonas*. Eukaryot Cell 7:555-9.
651 50. Füssy Z, Faitová T, Oborník M. 2019. Subcellular compartments interplay for carbon and nitrogen
652 allocation in *Chromera velia* and *Vitrella brassicaformis*. Genome Biol Evol 11:1765-1779.
653 51. Gerdes S, Lerma-Ortiz C, Frelin O, Seaver SM, Henry CS, de Crecy-Lagard V, Hanson AD. 2012.
654 Plant B vitamin pathways and their compartmentation: a guide for the perplexed. J Exp Bot 63:5379-
655 95.
656 52. Moffatt BA, Ashihara H. 2002. Purine and pyrimidine nucleotide synthesis and metabolism.
657 Arabidopsis Book 1:e0018.
658 53. Kořený L, Oborník M. 2011. Sequence evidence for the presence of two tetrapyrrole pathways in
659 *Euglena gracilis*. Genome Biol Evol 3:359-64.
660 54. Zimorski V, Rauch C, van Hellemond JJ, Tielens AGM, Martin WF. 2017. The mitochondrion of
661 *Euglena gracilis*, p 19-37. *In* Schwartzbach SD, Shigeoka S (ed), *Euglena*: Biochemistry, cell and
662 molecular biology, vol 979. Springer International Publishing, Cham.
663 55. Lambalot RH, Walsh CT. 1995. Cloning, overproduction, and characterization of the *Escherichia coli*
664 holo-acyl carrier protein synthase. J Biol Chem 270:24658-61.
665 56. Yuzawa Y, Nishihara H, Haraguchi T, Masuda S, Shimojima M, Shimoyama A, Yuasa H, Okada N,
666 Ohta H. 2012. Phylogeny of galactolipid synthase homologs together with their enzymatic analyses
667 revealed a possible origin and divergence time for photosynthetic membrane biogenesis. DNA Res
668 19:91-102.
669 57. Hori K, Nobusawa T, Watanabe T, Madoka Y, Suzuki H, Shibata D, Shimojima M, Ohta H. 2016.
670 Tangled evolutionary processes with commonality and diversity in plastidial glycolipid synthesis in
671 photosynthetic organisms. Biochim Biophys Acta 1861:1294-1308.

672 58. Li C, Wang Y, Liu L, Hu Y, Zhang F, Mergen S, Wang G, Schlappi MR, Chu C. 2011. A rice
673 plastidial nucleotide sugar epimerase is involved in galactolipid biosynthesis and improves
674 photosynthetic efficiency. PLoS Genet 7:e1002196.
675 59. Sun GL, Shen W, Wen JF. 2008. Triosephosphate isomerase genes in two trophic modes of
676 euglenoids (euglenophyceae) and their phylogenetic analysis. J Eukaryot Microbiol 55:170-7.
677 60. Markunas CM, Triemer RE. 2016. Evolutionary history of the enzymes involved in the Calvin-
678 Benson cycle in euglenids. J Eukaryot Microbiol 63:326-39.
679 61. Raines CA, Lloyd JC. 2001. C3 carbon reduction cycle, eLS doi:10.1038/npg.els.0001314. John
680 Wiley & Sons, Ltd.
681 62. Kiss JZ, Vasconcelos AC, Triemer RE. 1987. Structure of the euglenoid storage carbohydrate,
682 paramylon. Am J Bot 74:877-882.
683 63. Facchinelli F, Weber AP. 2011. The metabolite transporters of the plastid envelope: an update. Front
684 Plant Sci 2:50.
685 64. Haferkamp I, Deschamps P, Ast M, Jeblick W, Maier U, Ball S, Neuhaus HE. 2006. Molecular and
686 biochemical analysis of periplastidial starch metabolism in the cryptophyte *Guillardia theta*.
687 Eukaryot Cell 5:964-71.
688 65. Tabita FR, Hanson TE, Li H, Satagopan S, Singh J, Chan S. 2007. Function, structure, and evolution
689 of the RubisCO-like proteins and their RubisCO homologs. Microbiol Mol Biol Rev 71:576-99.
690 66. Pick TR, Brautigam A, Schulz MA, Obata T, Fernie AR, Weber AP. 2013. PLGG1, a plastidic
691 glycolate glycerate transporter, is required for photorespiration and defines a unique class of
692 metabolite transporters. Proc Natl Acad Sci U S A 110:3185-90.
693 67. Walker BJ, South PF, Ort DR. 2016. Physiological evidence for plasticity in glycolate/glycerate
694 transport during photorespiration. Photosynth Res 129:93-103.
695 68. Vogel A, Schwacke R, Denton AK, Usadel B, Hollmann J, Fischer K, Bolger A, Schmidt MH,
696 Bolger ME, Gundlach H, Mayer KFX, Weiss-Schneeweiss H, Temsch EM, Krause K. 2018.
697 Footprints of parasitism in the genome of the parasitic flowering plant *Cuscuta campestris*. Nat
698 Commun 9:2515.
699 69. Vollmer M, Thomsen N, Wiek S, Seeber F. 2001. Apicomplexan parasites possess distinct nuclear-
700 encoded, but apicoplast-localized, plant-type ferredoxin-NADP+ reductase and ferredoxin. J Biol
701 Chem 276:5483-90.
702 70. Schürmann P, Buchanan BB. 2008. The ferredoxin/thioredoxin system of oxygenic photosynthesis.
703 Antioxid Redox Signal 10:1235-74.
704 71. Figueroa-Martinez F, Nedelcu AM, Smith DR, Reyes-Prieto A. 2015. When the lights go out: the
705 evolutionary fate of free-living colorless green algae. New Phytologist 206:972-982.

72. Lohr M, Schwender J, Polle JE. 2012. Isoprenoid biosynthesis in eukaryotic phototrophs: a spotlight on algae. Plant Sci 185-186:9-22.
73. Waller RF, Gornik SG, Kořený L, Pain A. 2016. Metabolic pathway redundancy within the apicomplexan-dinoflagellate radiation argues against an ancient chromalveolate plastid. Commun Integr Biol 9:e1116653.
74. Cenci U, Qiu H, Pillonel T, Cardol P, Remacle C, Colleoni C, Kadouche D, Chabi M, Greub G, Bhattacharya D, Ball SG. 2018. Host-pathogen biotic interactions shaped vitamin K metabolism in Archaeplastida. Sci Rep 8:15243.
75. Seeger JW, Bentley R. 1991. Phylloquinone (vitamin K_1) biosynthesis in *Euglena gracilis* strain *Z*. Phytochemistry 30:3585-3589.
76. Fatihi A, Latimer S, Schmollinger S, Block A, Dussault PH, Vermaas WF, Merchant SS, Basset GJ. 2015. A dedicated type II NADPH dehydrogenase performs the penultimate step in the biosynthesis of vitamin K_1 in *Synechocystis* and *Arabidopsis*. The Plant Cell 27:1730-41.
77. Maeda H, DellaPenna D. 2007. Tocopherol functions in photosynthetic organisms. Curr Opin Plant Biol 10:260-5.
78. Brettel K. 1997. Electron transfer and arrangement of the redox cofactors in photosystem I. Biochimica et Biophysica Acta (BBA) - Bioenergetics 1318:322-373.
79. Furt F, Oostende Cv, Widhalm JR, Dale MA, Wertz J, Basset GJC. 2010. A bimodular oxidoreductase mediates the specific reduction of phylloquinone (vitamin K1) in chloroplasts. The Plant Journal 64:38-46.
80. Karamoko M, Cline S, Redding K, Ruiz N, Hamel PP. 2011. Lumen thiol oxidoreductase1, a disulfide bond-forming catalyst, is required for the assembly of photosystem II in *Arabidopsis*. The Plant Cell 23:4462.
81. Gu X, Harding S, Nyamdari B, Aulakh K, Clermont K, Westwood J, Tsai C-J. 2018. A role for phylloquinone biosynthesis in the plasma membrane as revealed in a non-photosynthetic parasitic plant. bioRxiv doi:10.1101/257519:257519.
82. Lochner K, Doring O, Bottger M. 2003. Phylloquinone, what can we learn from plants? Biofactors 18:73-8.
83. Schopfer P, Heyno E, Drepper F, Krieger-Liszkay A. 2008. Naphthoquinone-dependent generation of superoxide radicals by quinone reductase isolated from the plasma membrane of soybean. Plant Physiol 147:864.
84. Goddard-Borger ED, Williams SJ. 2017. Sulfoquinovose in the biosphere: occurrence, metabolism and functions. Biochem J 474:827-849.
85. Yoon EY, Yang AR, Park J, Moon SJ, Jeong EJ, Rho JR. 2017. Characterization of a new trioxilin

and a sulfoquinovosyl diacylglycerol with anti-inflammatory properties from the dinoflagellate *Oxyrrhis marina*. Mar Drugs 15:57.

86. Botté C, Saidani N, Mondragon R, Mondragon M, Isaac G, Mui E, McLeod R, Dubremetz JF, Vial H, Welti R, Cesbron-Delauw MF, Mercier C, Maréchal E. 2008. Subcellular localization and dynamics of a digalactolipid-like epitope in *Toxoplasma gondii*. J Lipid Res 49:746-62.
87. Botté CY, Yamaryo-Botté Y, Rupasinghe TW, Mullin KA, MacRae JI, Spurck TP, Kalanon M, Shears MJ, Coppel RL, Crellin PK, Maréchal E, McConville MJ, McFadden GI. 2013. Atypical lipid composition in the purified relict plastid (apicoplast) of malaria parasites. Proc Natl Acad Sci U S A 110:7506-11.
88. Donaher N, Tanifuji G, Onodera NT, Malfatti SA, Chain PS, Hara Y, Archibald JM. 2009. The complete plastid genome sequence of the secondarily nonphotosynthetic alga *Cryptomonas paramecium*: reduction, compaction, and accelerated evolutionary rate. Genome Biol Evol 1:439-48.
89. Sekiguchi H, Moriya M, Nakayama T, Inouye I. 2002. Vestigial chloroplasts in heterotrophic stramenopiles *Pteridomonas danica* and *Ciliophrys infusionum* (Dictyochophyceae). Protist 153:157-67.
90. Wicke S, Müller KF, de Pamphilis CW, Quandt D, Wickett NJ, Zhang Y, Renner SS, Schneeweiss GM. 2013. Mechanisms of functional and physical genome reduction in photosynthetic and nonphotosynthetic parasitic plants of the broomrape family. The Plant Cell 25:3711.
91. Kim GH, Jeong HJ, Yoo YD, Kim S, Han JH, Han JW, Zuccarello GC. 2013. Still acting green: continued expression of photosynthetic genes in the heterotrophic Dinoflagellate *Pfiesteria piscicida* (Peridiniales, Alveolata). PLoS One 8:e68232.
92. Schwender J, Goffman F, Ohlrogge JB, Shachar-Hill Y. 2004. Rubisco without the Calvin cycle improves the carbon efficiency of developing green seeds. Nature 432:779-82.
93. Iddar A, Valverde F, Serrano A, Soukri A. 2003. Purification of recombinant non-phosphorylating NADP-dependent glyceraldehyde-3-phosphate dehydrogenase from *Streptococcus pyogenes* expressed in *E. coli*. Mol Cell Biochem 247:195-203.
94. Rius SP, Casati P, Iglesias AA, Gomez-Casati DF. 2006. Characterization of an *Arabidopsis thaliana* mutant lacking a cytosolic non-phosphorylating glyceraldehyde-3-phosphate dehydrogenase. Plant Mol Biol 61:945-57.
95. Tucci S, Vacula R, Krajčovič J, Proksch P, Martin W. 2010. Variability of wax ester fermentation in natural and bleached *Euglena gracilis* strains in response to oxygen and the elongase inhibitor flufenacet. J Eukaryot Microbiol 57:63-9.
96. Yoshida Y, Tomiyama T, Maruta T, Tomita M, Ishikawa T, Arakawa K. 2016. De novo assembly and comparative transcriptome analysis of *Euglena gracilis* in response to anaerobic conditions.

BMC Genomics 17:182.

97. Roger AJ, Muñoz-Gómez SA, Kamikawa R. 2017. The origin and diversification of mitochondria. Curr Biol 27:R1177-R1192.
98. Jones P, Binns D, Chang HY, Fraser M, Li W, McAnulla C, McWilliam H, Maslen J, Mitchell A, Nuka G, Pesseat S, Quinn AF, Sangrador-Vegas A, Scheremetjew M, Yong SY, Lopez R, Hunter S. 2014. InterProScan 5: genome-scale protein function classification. Bioinformatics 30:1236-40.
99. Mistry J, Finn RD, Eddy SR, Bateman A, Punta M. 2013. Challenges in homology search: HMMER3 and convergent evolution of coiled-coil regions. Nucleic Acids Res 41:e121.
100. Ebenezer TE, Carrington M, Lebert M, Kelly S, Field MC. 2017. *Euglena gracilis* genome and transcriptome: Organelles, nuclear genome assembly strategies and initial features. Adv Exp Med Biol 979:125-140.
101. Keeling PJ, Burki F, Wilcox HM, Allam B, Allen EE, Amaral-Zettler LA, Armbrust EV, Archibald JM, Bharti AK, Bell CJ, Beszteri B, Bidle KD, Cameron CT, Campbell L, Caron DA, Cattolico RA, Collier JL, Coyne K, Davy SK, Deschamps P, Dyhrman ST, Edvardsen B, Gates RD, Gobler CJ, Greenwood SJ, Guida SM, Jacobi JL, Jakobsen KS, James ER, Jenkins B, John U, Johnson MD, Juhl AR, Kamp A, Katz LA, Kiene R, Kudryavtsev A, Leander BS, Lin S, Lovejoy C, Lynn D, Marchetti A, McManus G, Nedelcu AM, Menden-Deuer S, Miceli C, Mock T, Montresor M, Moran MA, Murray S, et al. 2014. The Marine Microbial Eukaryote Transcriptome Sequencing Project (MMETSP): illuminating the functional diversity of eukaryotic life in the oceans through transcriptome sequencing. PLoS Biol 12:e1001889.
102. Katoh K, Standley DM. 2013. MAFFT multiple sequence alignment software version 7: improvements in performance and usability. Mol Biol Evol 30:772-80.
103. Capella-Gutierrez S, Silla-Martinez JM, Gabaldon T. 2009. trimAl: a tool for automated alignment trimming in large-scale phylogenetic analyses. Bioinformatics 25:1972-3.
104. Goodstadt L, Ponting CP. 2001. CHROMA: consensus-based colouring of multiple alignments for publication. Bioinformatics 17:845-6.
105. Nguyen LT, Schmidt HA, von Haeseler A, Minh BQ. 2015. IQ-TREE: a fast and effective stochastic algorithm for estimating maximum-likelihood phylogenies. Mol Biol Evol 32:268-74.
106. Cramer M, Myers J. 1952. Growth and photosynthetic characteristics of *Euglena gracilis*. Archiv Mikrobiol 17:384-402.
107. Sonneborn TM. 1950. Methods in the general biology and genetics of *Paramecium aurelia*. Journal of Experimental Zoology 113:87-147.
108. Tomčala A, Kyselová V, Schneedorferová I, Opekarová I, Moos M, Urajová P, Kručinská J, Oborník M. 2017. Separation and identification of lipids in the photosynthetic cousins of Apicomplexa

Chromera velia and *Vitrella brassicaformis*. J Sep Sci 40:3402-3413.

109. Folch J, Lees M, Sloane Stanley GH. 1957. A simple method for the isolation and purification of total lipides from animal tissues. J Biol Chem 226:497-509.

110. Botté CY, Yamaryo-Botté Y, Janouškovec J, Rupasinghe T, Keeling PJ, Crellin P, Coppel RL, Maréchal E, McConville MJ, McFadden GI. 2011. Identification of plant-like galactolipids in *Chromera velia*, a photosynthetic relative of malaria parasites. J Biol Chem 286:29893-903.

FIGURE LEGENDS

Figure 1: IPP and terpenoid-quinone biosynthesis in *E. longa* and its phototrophic relative *E. gracilis*. a: Schematic comparison of the localization and evolutionary origin of enzymes (see colour-coding graphical legend below the "cells"). Abbreviations, IPP synthesis: ACAT – acetyl-CoA acetyltransferase, CDP-ME – 4-(cytidine 5'-diphospho)-2-C-methyl-D-erythritol, CDP-MEP – 2-phospho-CDP-ME, CMK – CDP-ME kinase, CMS – CDP-ME synthase, DMAPP – dimethylallyl diphosphate, DXP – 1-deoxy-D-xylulose 5-phosphate, DXR – DXP reductase, DXS – DXP synthase, FPP – farnesyl siphosphate synthase, GGPS – geranylgeranyl-diphosphate synthase, HDR – HMB-PP reductase, HDS – HMB-PP synthase, HMB-PP – 4-hydroxy-3-methylbut-2-en-1-yl diphosphate, HMG-CoA – 3-hydroxy-3-methylglutaryl-CoA, HMGCR – HMG-CoA reductase, HMGCS – HMG-CoA synthase, IDI – isopentenyl-diphosphate delta-isomerase, MCS – MEcPP synthase, MDD – mevalonate-diphosphate decarboxylase, MEcPP – 2-C-methyl-D-erythritol 2,4-cyclodiphosphate, MEP – 2-C-methyl-D-erythritol 4-phosphate, MVK – mevalonate kinase, PMVK – phosphomevalonate kinase, PPS – unspecified polyprenyl-diphosphate synthase, ? – unclear substrate; Terpenoid-quinone synthesis: 4HPP – 4-hydroxyphenylpyruvate, HPD – hydroxyphenylpyruvate dioxygenase, HPT – homogentisate phytyltransferase, MMT – MPBQ/MPSQ methyltransferase, TAT – tyrosine aminotransferase, TC – tocopherol cyclase, TMT – tocopherol-O-methyltransferase, VTE5 – phytyl kinase, VTE6 – phytyl-phosphate kinase. **b:** MS/MS spectrum record of *E. longa* α-tocopherol and the proposed fragmentation pattern in positive ionization mode (inset). Monoisotopic masses of particular fragments were obtained by simulation in Xcalibur software. **c:** Semiquantitative comparison of tocopherol species in *E. longa*, heterotrophically (dark) grown *E. gracilis* and autotrophically grown *E. gracilis*. **d-e:** MS/MS spectrum record of *E. longa* 5-hydroxyphylloquinone and the proposed fragmentation pattern in positive ionization mode (inset); semiquantitative comparison of 5-hydroxyphylloquinone in *E. longa*, heterotrophically (dark) grown *E. gracilis* and autotrophically grown *E. gracilis*.

Figure 2: Fatty acid and lipid biosynthesis in *E. longa* and *E. gracilis*. a: Schematic comparison of the localization and evolutionary origin of enzymes. Abbreviations, fatty acid synthesis: ACC – acetyl-CoA

carboxylase, ACS – acetyl-CoA synthetase, ENR – enoyl-CoA reductase, Fas1 – malonyl-CoA/acetyl-CoA: ACP transacylase, FASI – type I fatty acid synthase, FAT – fatty acyl-ACP thioesterase, HD – hydroxyacyl-ACP dehydratase, KAR – ketoacyl-ACP reductase, KAS – ketoacyl-ACP synthase, TE – fatty acid thioesterase, TRX – thioredoxin-regulated enzyme; glycolipid synthesis: AAS – acyl-ACP synthase, ACPS – holo-ACP synthase, AGP-AT – acylglycerophosphate acyltransferase, G3P-AT – glycerol-3-phosphate acyltransferase, G3PDH – glycerol-3-phosphate dehydrogenase, MGDG/DGDG – mono-/digalactosyl diacylglycerol, MGDGS/DGDGS – MGDG/DGDG synthase, PAP – phosphatidic acid phosphatase, SQD1 – UDP-sulfoquinovose synthase, SQD2/SQDX – sulfoquinovosyl diacylglycerol (SQDG) synthase, UGE/PHD1 – UDP-glucose epimerase, USPP – UDP-sugar pyrophosphorylase; phospholipid synthesis: CDS – CDP-diacylglycerol synthase, PGP1 – phosphatidylglycerophosphate synthase, PGP-P – phosphateidylglycerophosphate phosphatase. **b:** Semiquantitative comparison of glycolipids present in *E. longa* and autotrophically grown *E. gracilis*. Note the logarithmic scale of the quantification units (peak area). Peak area is an arbitrary unit expressing the intensity of the signal of a particular lipid species, recalculated according to their respective ionization promptitude. As each lipid species have different ionization promptitude, note that direct comparison can be done only within lipid class (for details, see Tomčala et al. 2017). **c-e:** Immunofluorescence micrographs using anti-DGDG antibody (C), DAPI (D) and differential interference contrast (E). Autotrophic *E. gracilis* represents a positive control, while the aplastidic euglenozoan *R. costata* was used as negative control.

Figure 3: Euglenophytes have replaced the eukaryotic form of sulfoquinovosyltransferase (SQD2) with a bacterial version (SqdX). The maximum-likelihood tree was inferred with IQ-TREE using the LG+F+G4 substitution model and ultra-fast bootstrapping. The UFboot support values are indicated at branches when higher than 75%. Accession numbers of sequences included in the analysis are provided in Table S11.

Figure 4: Carbon metabolism in the plastids of *E. longa* and *E. gracilis*. a: The Calvin-Benson cycle (CBC) resident to this organelle is central to the plastid carbon metabolism, regulated by the ferredoxin/thioredoxin (Fd/Trx) system. Reduction of disulfide bonds by the Fd/Trx system activates FBP and PRK. FTR and FD of the Fd/Trx system require for their function a post-translationally added Fe-S prosthetic group provided by the Fe-S assembly system. GapN apparently mediates shuttling of reducing equivalent (NADPH) through the exchange of DHAP/GA3P and 3PG, reflecting the cytosolic NADPH/$NADP^+$ ratio and thus an overall metabolic state of the cell. In contrast, *E. gracilis* plastid is an energy-converting organelle, harvesting light into chemical energy bound as NADPH and ATP and subsequently using this bound energy to fix CO_2 into organic carbohydrates via the CBC. Enzyme

abbreviations are colour-coded according to their inferred evolutionary origin, see the graphical legend. **b:** Stoichiometric comparison of reactions converting glyceraldehyde 3-phosphate to 3-phosphoglycerate via glycolysis and the Calvin-Benson pathway. Abbreviations: 3PG – 3-phosphoglycerate, ALDO – aldolase, DHAP – dihydroxyacetone-phosphate, FBP – fructose-1,6-bisphosphatase, GA3P – glyceraldehyde-3-phosphate, GAPDH – glyceraldehyde-3-phosphate dehydrogenase, PGK – 3-phosphoglygerate kinase, PGP – phosphoglycolate phosphatase, PLGG1 – plastid glycolate/glycerate transporter, PRK – phosphoribulokinase, RBCL/RBCS – RuBisCO large/small subunit, RCA – RuBisCO activase, RPE – ribulose-5-phosphate epimerase; RPIA – ribulose-phosphate isomerase A, SBP – sedoheptulose-1,7-bisphosphatase, TKTL – transketolase, TPI – triose-phosphate isomerase, TPT – triose-phosphate translocator; Fd/Trx system: FD – ferredoxin; FNR – FD/NADP+ oxidoreductase, FTR – FD/TRX oxidoreductase, TRX – thioredoxin, ATPS – ATP synthase, ATPC – ADP/ATP translocase, LHC – light-harvesting complex.

Figure 5: The inferred phylogeny of FNR. The maximum-likelihood tree was inferred with IQ-TREE using the LG+F+G4 substitution model and ultra-fast bootstrapping. The UFboot support values are indicated at branches when higher than 75%. Euglenophyte species are in bold, and their putative photosynthetic and non-photosynthetic homologs are depicted. The two forms of plant FNR are indicated: P, photosynthetic; NP, non-photosynthetic. Accession numbers of sequences included in the analysis are provided in Table S12.

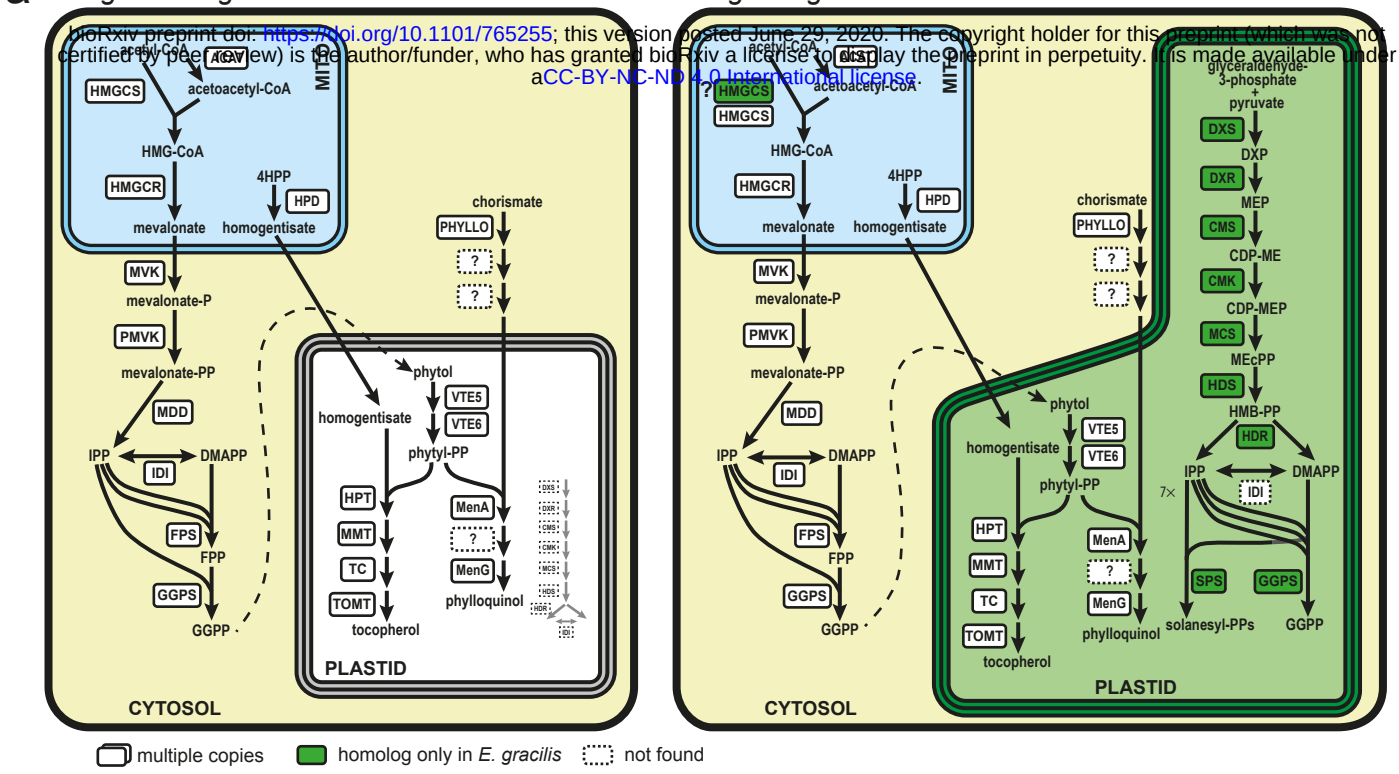

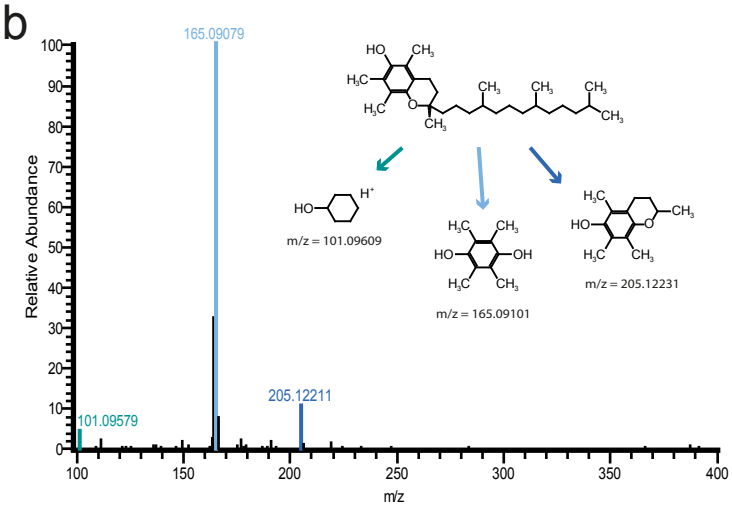

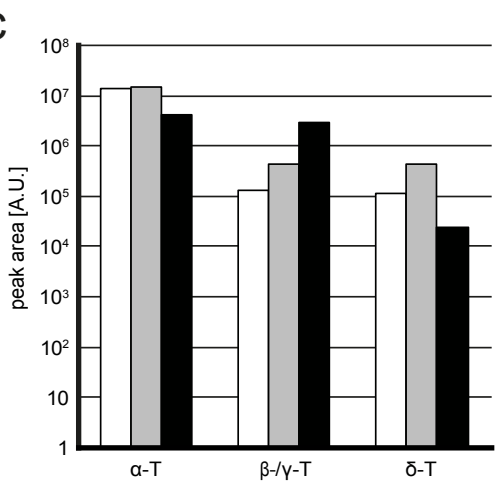

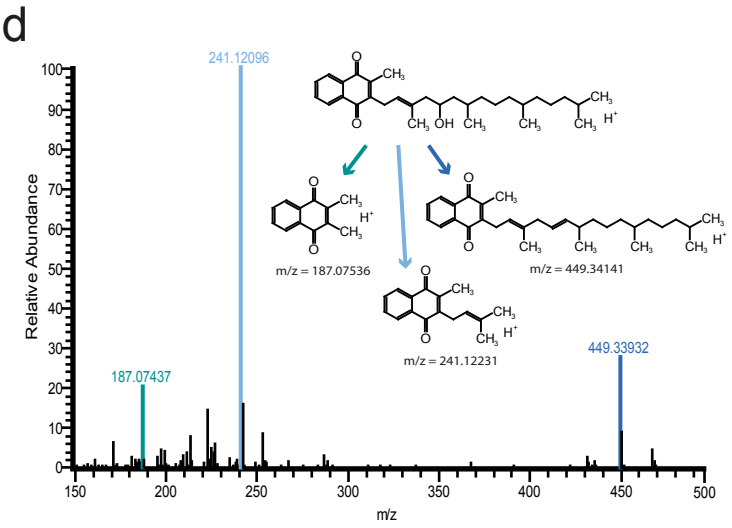

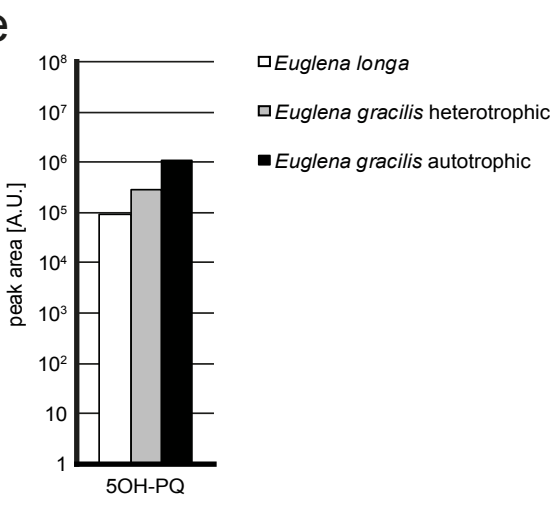

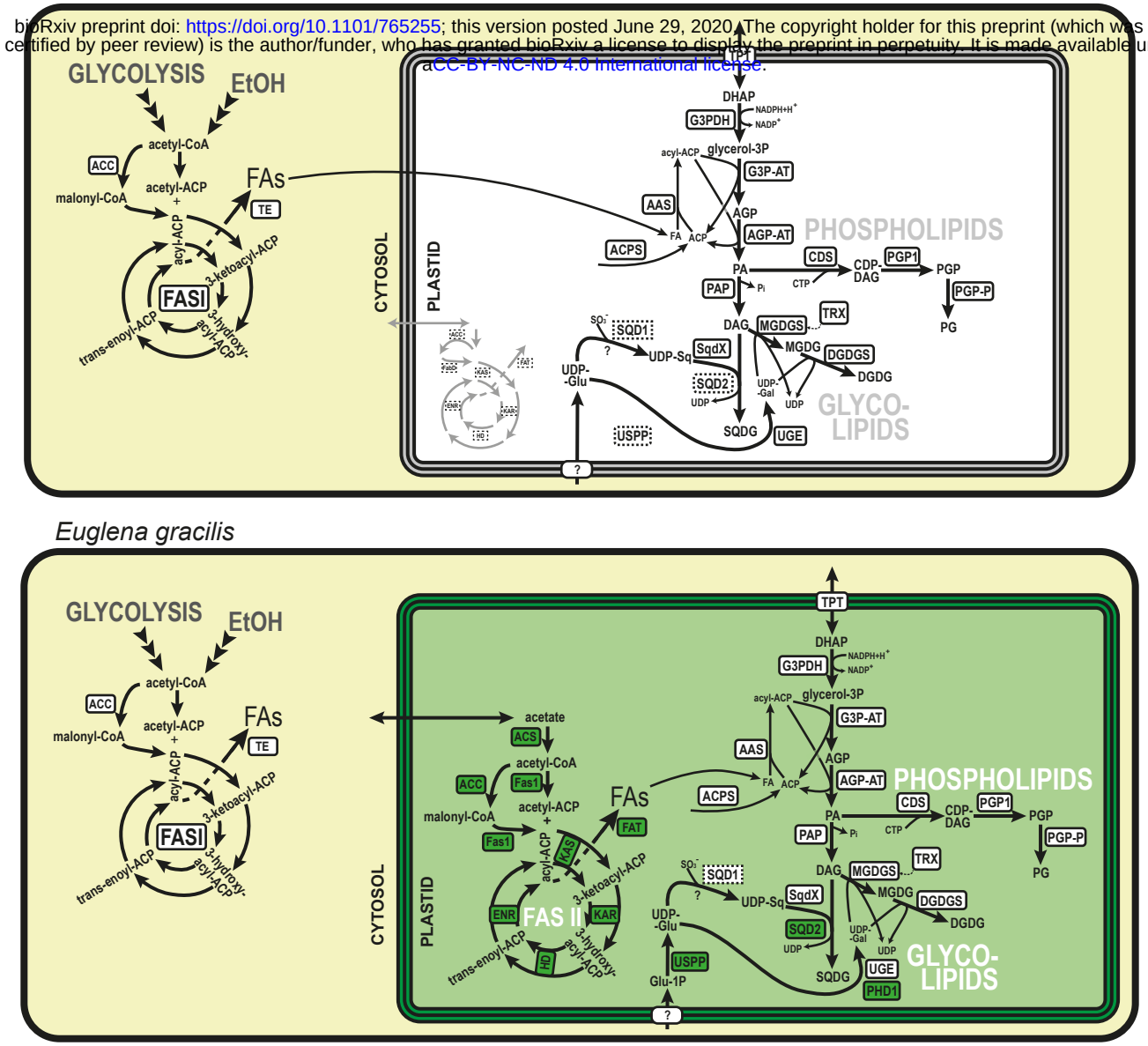

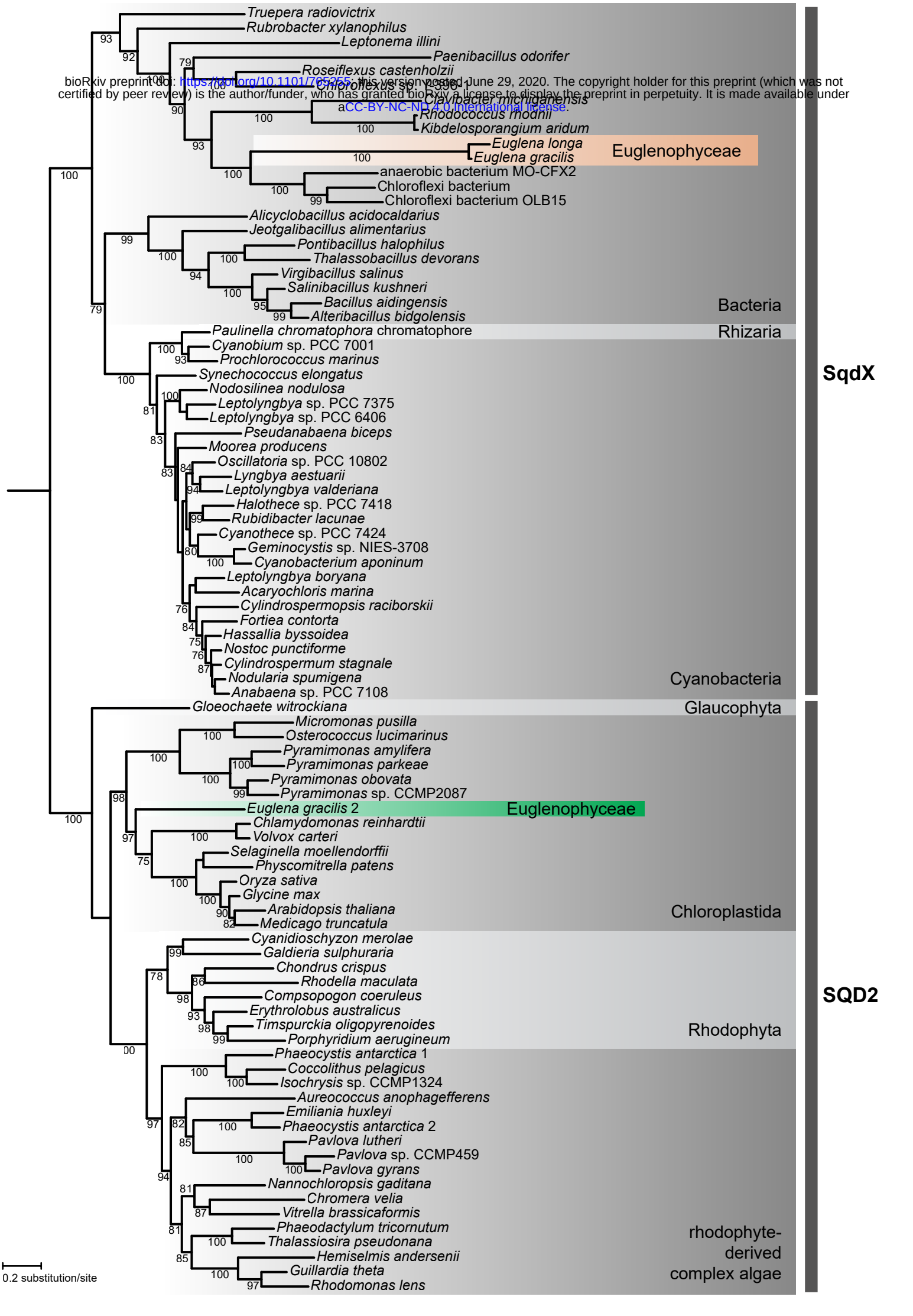

a

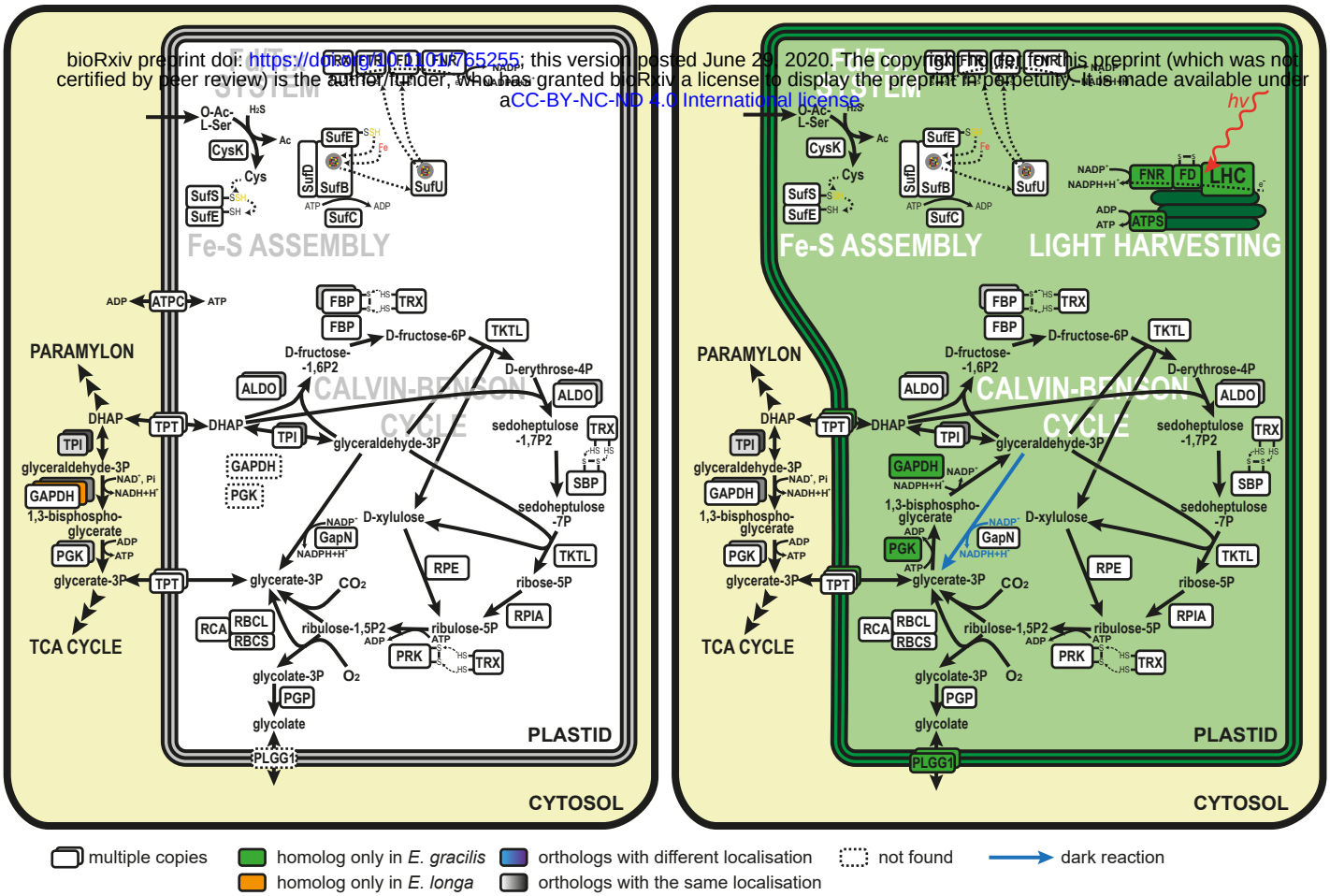

b

glycolysis: $5\ GA3P + 5\ NAD^+ + 5\ ADP + 5\ PO_3^{2-} \rightarrow 5\ 3PG + 5\ NADH + 5\ H^+ + 5\ ATP$

CB pathway: $5\ GA3P + 3\ CO_2 + 3\ H_2O + 3\ ATP \rightarrow 6\ 3PG + 3\ ADP + 2\ PO_3^{2-}$